

PHYSICAL REVIEW B

CONDENSED MATTER

THIRD SERIES, VOLUME 42, NUMBER 14

15 NOVEMBER 1990-I

Optical properties and electronic structures of the intermetallic compounds AuGa₂ and PtGa₂

Kwang Joo Kim, B. N. Harmon, Liang-Yao Chen,* and David W. Lynch

Department of Physics and Ames Laboratory, U.S. Department of Energy, Iowa State University, Ames, Iowa 50011

(Received 8 May 1990; revised manuscript received 30 July 1990)

The electronic structures of AuGa₂ and PtGa₂ have been studied with use of spectroscopic ellipsometry and the dielectric functions have been determined in the 1.2–5.5-eV region. Both compounds show interband absorption at low photon energies (< 1.3 eV). The interband absorption for AuGa₂ is strong at about 2 eV while that for PtGa₂ shows a broad structure in the range 2.5–4.5 eV, with a shoulder at 3.3 eV. The observed interband features in ϵ_2 can be interpreted in terms of self-consistent relativistic band-structure calculations using the linear augmented-plane-wave method. The interband contribution to the imaginary part of the dielectric function ϵ_2^i has been calculated including the effect of the electric dipole matrix elements. The overall agreement is good between the band calculations and the ellipsometry results in the 1.2–5.5-eV region for both the magnitude and the positions of the structures. Below 1.2 eV the calculational results for both compounds show interband absorption, which is also qualitatively suggested by the ellipsometry results.

I. INTRODUCTION

The binary intermetallic compounds AuGa₂ and PtGa₂ have the cubic fluorite (CaF₂) structure in which Au or Pt atoms form a fcc sublattice and the Ga atoms occupy the tetrahedral sites located one-quarter of the way up the body diagonals. Earlier studies of the electrical properties of AuGa₂, AuAl₂, and AuIn₂ (Ref. 1) showed that they are good metallic conductors with room-temperature conductivities about one-fifth that of Cu. Also, Fermi-surface studies on these compounds^{2,3} indicated that they behave nearly-free-electron-like to some extent. Optical reflectivities were measured on these compounds^{4,5} and dielectric functions were calculated by using Kramers-Kronig (KK) analyses. Chen and Lynch⁶ measured the complex dielectric functions of AuAl₂ and PtAl₂ by spectroscopic ellipsometry. Using published band structures of the compounds⁷ they were able to assign some interband transitions to the structures observed in the dielectric functions.

As is well known, the electronic band structure of Au (Refs. 8–10) is characterized by narrow 5*d* bands which hybridize significantly with the *s-p* bands around the Brillouin-zone boundary. Also, the spin-orbit interaction splits the 5*d* states into states with $j = \frac{3}{2}$ and $j = \frac{5}{2}$. This ordering combines with crystal-field effects so that at the Γ point, the spin-orbit and crystal-field interactions cause the fourfold $j = \frac{3}{2}$ states (upper Γ_8^+) to shift to higher energy and the $j = \frac{5}{2}$ states to split into fourfold (lower Γ_8^+) and twofold (Γ_7^+) levels. The spin-orbit interaction

enhances the *d*-band width, and the energy gap between the $j = \frac{5}{2}$ levels at the Γ point is about 1 eV for Au, a gap large enough to be detected in photoemission measurements.^{11,12}

In AuGa₂, according to the earlier band calculations on this compound,^{7,13} the width of the Au-derived 5*d* bands is narrower than that of elemental Au because by forming a compound with Ga the distances between Au atoms become approximately 1.5 times larger than in elemental Au which results in weaker *d-d* overlap interactions between Au atoms. Also, the lowest-lying *s* band reaches the zone boundary (e.g., X_1) without crossing the *d* bands. This results in less *s-d* hybridization and the *d* bands reside within a band gap between *s* and *p* bands. Therefore, in AuGa₂, the electronic states near the Fermi level E_F are expected to have mostly *s-p* character of both constituents and the interband transitions between them are expected to contribute to the low-energy (< 5 eV) optical properties of the compound. This is in contrast to the case for pure Au which has interband contributions below 5 eV involving the *d* bands^{14,15} which extend higher in energy compared to those of AuGa₂. The electronic properties of PtGa₂,¹⁶ on the other hand, are not so well studied as those of AuGa₂. However, we can at least estimate the qualitative differences in the electronic structure between PtGa₂ and Pt based on those between AuGa₂ and Au.

The electronic structure information gained from optical measurements comes from the spectral dependence of the optical response described by the complex dielectric

function which involves the characteristic energies of prominent excitations, the joint density of states, and the relative oscillator strengths of the excitations. The complex dielectric function of a metal can be described as the sum of an intraband term and an interband term,

$$\tilde{\epsilon} = \tilde{\epsilon}^f + \tilde{\epsilon}^b. \quad (1)$$

The intraband term of the optical spectra can be treated quantitatively within the framework of the Drude model as

$$\epsilon_1^f = 1 - \frac{\omega_p^2 \tau^2}{1 + \omega^2 \tau^2}, \quad (2)$$

$$\epsilon_2^f = \frac{\omega_p^2 \tau}{\omega(1 + \omega^2 \tau^2)}. \quad (3)$$

The two parameters of the model are $\omega_p^2 (=4\pi N e^2 / m^*)$, the bulk plasma frequency squared, and τ^{-1} , the electron scattering rate. The interband term depends upon the details of the electronic band structure. It is related to momentum-conserving electric dipole transitions between states separated by the photon energy.

In this work, we report ellipsometric measurements of the dielectric functions of AuGa₂ and PtGa₂ in the 1.2–5.5-eV region which we interpret in terms of intraband and interband transitions. We also performed self-consistent band calculations for both compounds using the linearized augmented-plane-wave (LAPW) method. The calculations were done semirelativistically including the spin-orbit interaction as a perturbation.¹⁷ Using the calculated one-electron eigenfunctions, we calculated the electric dipole matrix elements for the direct interband transitions between the occupied $|i\rangle$ and the unoccupied $|f\rangle$ states \mathbf{P}_{fi} , given by

$$\mathbf{P}_{fi} = \frac{\hbar}{\Omega i} \langle f | \nabla | i \rangle \quad (4)$$

integrated over the unit cell of volume Ω . These are related to the interband contribution to the imaginary part of the complex dielectric function ϵ_2^b by

$$\epsilon_2^b = \frac{4\pi^2 e^2}{3m^2 \omega^2} \sum_{f,i} \int_{\text{BZ}} d^3k \frac{2}{(2\pi)^3} |\mathbf{P}_{fi}|^2 \delta(E_f - E_i - \hbar\omega), \quad (5)$$

which is to be compared with the experimental results. We did not include the spin-flip terms of the relativistic matrix elements as they are expected to be small.¹⁸

II. EXPERIMENTAL

The raw materials used in this work were bulk Au, Pt, and Ga, all 99.99% purity. The AuGa₂ sample is a polycrystal made by arc melting in an argon atmosphere. The weight loss during melting did not exceed 0.1%. The PtGa₂ sample is a single crystal which is stable at room temperature. It was grown by the Bridgman method which is described in detail elsewhere,¹⁹ oriented using Laue x-ray diffractometry, then cut to reveal a (111) surface. The AuGa₂ sample has a slight bluish hue and the PtGa₂ sample is a yellow color like that of gold.

The lattice parameters obtained by x-ray-diffraction

measurements are 6.036 Å for AuGa₂ and 5.911 Å for PtGa₂, which are in good agreement with the values in the literature.^{13,16} Before the measurement, the samples were mechanically polished with abrasives, the final grade being a paste of 0.05- μm -diam alumina, and afterwards cleaned by acetone and methanol.

The scanning photometric ellipsometer with rotating polarizer and analyzer, which has been discussed in detail previously,²⁰ was used to determine the dielectric functions of the samples at room temperature. Measurements were made in the 1.2–5.5-eV range at energy intervals of 0.01 eV in the 1.2–2.5-eV range and 0.02 eV in the 2.5–5.5-eV range. The spectral bandpass was 3.3 nm and the measurement errors did not exceed 1% in ϵ_2 . Systematic errors caused by oxide overlayer formation appear to be small. Such errors can cause a small shift in the absolute values of the spectra but do not alter the positions of the spectral features.

III. BAND-CALCULATIONAL DETAILS

The crystal structure of AuGa₂ and PtGa₂ is cubic fluorite (CaF₂). The Bravais lattice is fcc, the space group is O_h^5 ($Fm\bar{3}m$), and this structure has three atoms per unit cell. The lattice constants are 6.06 Å for AuGa₂ and 5.91 Å for PtGa₂.

Electronic band-structure calculations for both compounds were performed using the LAPW method, employing the standard muffin-tin approximation for the crystal potential, which provides a good approximation for a cubic close-packed structure. The calculations were scalar relativistic,¹⁷ in which the Dirac equation is reduced to omit initially the spin-orbit interaction (thus keeping spin as a good quantum number but retaining all other relativistic kinematic effects). The spin-orbit interaction is added perturbatively after the semirelativistic bands and wave functions have been obtained.

The starting muffin-tin crystal potentials were constructed from the superposition of neutral atomic charge densities obtained from self-consistent atomic calculations by the Dirac-Slater method using a variation of the Liberman-Waber-Cromer program,²¹ which includes relativistic effects. The atomic configurations of Au and Ga were $5d^{10}6s^1$ and $4s^2 4p^1$, respectively, in AuGa₂ and those of Pt and Ga were $5d^9 6s^1$ and $4s^2 4p^1$, respectively, in PtGa₂. The exchange-correlation contribution to the potential was calculated by using the local-density approximation of Hedin and Lundqvist²² to the density-functional formalism. This local-density potential has the advantage of being self-consistent and containing no adjustable parameters and has proved successful in accounting for the ground-state properties of a variety of metals.^{23–26} The crystal charge density was calculated from the wave functions of the filled states obtained by solving the Hamiltonian containing the effective crystal potential. By mixing the new charge density with the old charge density we can construct the new potential from this mixture and the self-consistency procedure was continued until the change in the charge in each muffin-tin sphere converged to within 10^{-4} electron and the energy eigenvalues to within 10^{-4} Ry in successive iterations.

The muffin-tin sphere radii were chosen so that the spheres surrounding the Au and Pt sites extended 57% and 56%, respectively, of the way up to the Ga site. With this arrangement only 47% of the unit-cell volume is occupied by the three muffin-tin spheres for both compounds. In other words, the crystal potential is taken as constant over 53% of the unit-cell volume. This is a questionable approximation to the real crystal potential. This problem of approximating the potential as a constant in a large region can be alleviated by including more of the unit-cell volume inside an additional sphere. This is accomplished by considering one additional sphere at the unoccupied octahedral site (one-half of the way up the body diagonal and between the Ga atoms). The size of this sphere is taken to be as large as possible without changing the sizes of the other spheres. The radii of the spheres are listed in Table I. By including this sphere the amount of the unit-cell volume enclosed within the muffin-tin sphere becomes 70% for AuGa₂ and 71% for PtGa₂. Although no nucleus is at the center of the added sphere, upon self-consistency it contains 0.70 electron for AuGa₂ and 0.66 electron for PtGa₂.

The size of the LAPW basis-function set for each calculation was set to satisfy $K_{\max}R_{\text{MT}}=7.5$ for the smallest muffin-tin radius R_{MT} . This yielded about 170–200 LAPW's for both compounds. Inside R_{MT} , the wave functions were expanded in terms of spherical harmonics of angular momentum up to $l=12$. There were 46 \mathbf{k} points in the $\frac{1}{48}$ th of the Brillouin zone included for the self-consistent iterations.

We also calculated the density of states (DOS) for both compounds. We used the energy eigenvalues for the first 13 bands at 152 \mathbf{k} points. They were least-squares-fitted with 81 symmetrized plane waves (the typical rms error of the fits was less than 1 mRy). These fits were used to generate the band energies at the corners of 2048 small tetrahedra which filled the irreducible wedge ($\frac{1}{48}$) of the Brillouin zone. The DOS was then obtained using the linear-energy-tetrahedron method²⁷ which was also used to calculate the interband contribution to the imaginary part of the dielectric function ϵ_2^b . In calculating ϵ_2^b as in Eq. (5), we needed to compute the electric dipole matrix elements as in Eq. (4). The energy eigenvalues were evaluated at the four corners of 110 elementary tetrahedra in the irreducible $\frac{1}{48}$ th of the Brillouin zone and the electric dipole matrix elements were calculated using the wave functions at the centers of the tetrahedra. We assumed the electric dipole matrix elements to be constant within any one tetrahedron, and equal to the matrix element calculated at the center of the tetrahedron.

TABLE I. Parameters used in the band calculations.

	AuGa ₂	PtGa ₂
Lattice constant (Å)	6.06	5.91
Muffin-tin radius (Å)	Au 1.50 Ga 1.13	Pt 1.43 Ga 1.13

IV. RESULTS AND DISCUSSION

A. Optical properties

The real and imaginary parts of the measured complex dielectric functions of AuGa₂ and PtGa₂ in the 1.2–5.5-eV range are shown in Fig. 1. For AuGa₂, the imaginary part of the dielectric function ϵ_2 shows a broad structure at around 2 eV due to interband absorption. For PtGa₂, a structure in ϵ_2 due to interband absorption starts at about the same energy as in AuGa₂ but it is weaker in intensity. We also can see a broad structure peaked at about 3.3 eV in PtGa₂. Figure 2 shows the normal-incidence reflectivities of AuGa₂ and PtGa₂ calculated from their dielectric functions. For both compounds the reflectivities at low energies (<2 eV) are rather small compared to those of the noble metals in the same energy range. The reflectivity of AuGa₂ decreases to a minimum at 1.90 eV where its value of less than 60% agrees well with other results.^{4,5} This is due to an onset of interband transitions around that energy. The reflectivity increases towards a maximum of about 70% at about 3.1 eV after which it decreases slowly. By comparing the reflectivities of AuGa₂ and AuAl₂ (Refs. 4–6) we can see that the reflectivity of AuGa₂ is smaller than that of AuAl₂ at lower energies (<2 eV) but larger at higher energies (2–5 eV) and the reflectivity minimum of AuAl₂ is located at higher energy (≈ 2.2 eV). The reflectivity of PtGa₂ decreases to a minimum of less than 40% at 2.92 eV, then it slowly increases to a maximum at about 4.0 eV, after which it decreases slowly. We also can see a similarity between the reflectivities of PtGa₂ and PtAl₂, in which both have minima at about 3 eV and shoulders at about 4 eV, as a result of which they exhibit a yellow color.²⁸

To estimate the interband contribution to the imaginary part of the dielectric function ϵ_2^b quantitatively from our optical data, we need to subtract the intraband contribution ϵ_2^f from the measured ϵ_2 . By assuming that the optical properties of these compounds are governed by intraband transitions of the quasifree conduction electrons at low energies (here less than 0.5 eV), we can fit the low-energy behavior of the dielectric function to the Drude model if we have the dielectric functions at low

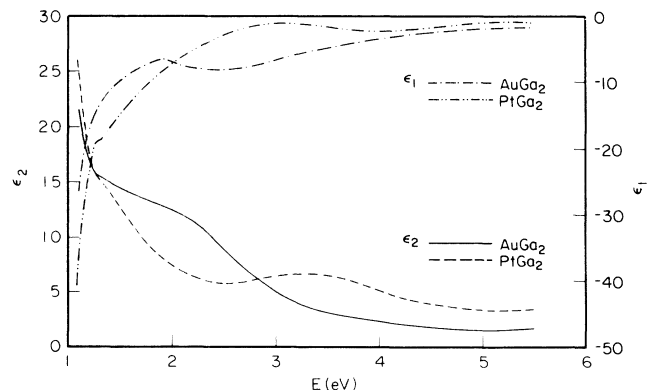


FIG. 1. Real and imaginary parts of the complex dielectric functions of AuGa₂ and PtGa₂.

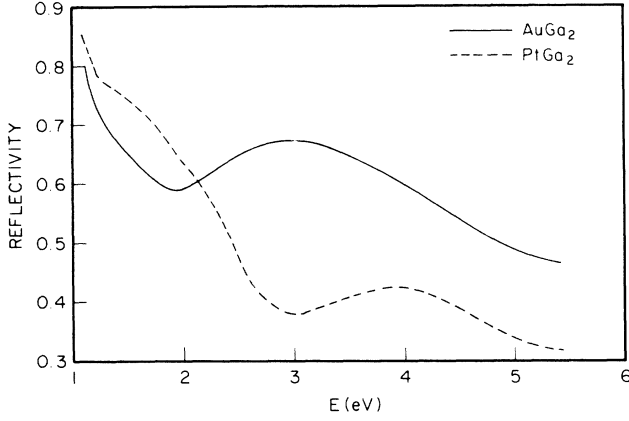


FIG. 2. Normal-incidence reflectivity spectra of AuGa₂ and PtGa₂. Note that the zero of the reflectivity is suppressed.

energies for both compounds. This assumption has been a good approximation for noble metals. Then we can obtain the free-electron (Drude) parameters for both compounds which can be used to estimate the intraband contributions at higher energies.

We obtained the dielectric functions at low energies (<1 eV) by KK analyses of the reflectivity data in the 0.02–6.2-eV range measured by Wieliczka *et al.*²⁹ at room temperature for both compounds. For energies larger than 6.2 eV and up to 100 eV reflectivities were assumed to drop off as ω^{-p} , and for still higher energies as ω^{-4} , where p (<4) is an adjustable parameter to make the calculated dielectric functions agree in magnitude with the ellipsometry data in the 1.2–5.5-eV region. The structure of the spectra is not sensitive to values of p .

In estimating the Drude parameters we assume that $\tilde{\epsilon} \approx \tilde{\epsilon}^f$ for the dielectric functions at low energies (<0.5 eV) obtained from KK analyses of the reflectivity data for both compounds, which means we neglect the contributions from interband absorption at low energies. We also assume that $\omega\tau \gg 1$ at the same energy range which has been a good approximation for noble metals. For AuGa₂,¹ the dc relaxation time τ_{dc} was estimated to be 8.0×10^{-14} sec from the dc resistivity, so that the above condition is satisfied at 0.5 eV. Then Eqs. (2) and (3) reduce, respectively, to

$$\epsilon_1 = \epsilon_\infty - \frac{\omega_p^2}{\omega^2}, \quad (6)$$

$$\epsilon_2 = \frac{\omega_p^2}{\omega^3 \tau}, \quad (7)$$

where $\epsilon_\infty = 1 + \epsilon_1^b$ with ϵ_1^b the contribution to ϵ_1 from interband transitions at higher energies.

By linear-regression fitting of the real part of the dielectric functions below 0.5 eV we can obtain ϵ_∞ and ω_p . Also, it is known that in order to fit the low-energy optical spectra for a variety of metals τ needs to be frequency dependent.^{30,31} For the noble metals, it is empirically given by^{32,33}

$$\tau^{-1} = \tau_0^{-1} + \beta \omega^2, \quad (8)$$

and we used this relation to fit the imaginary parts of the dielectric functions below 0.5 eV to get τ_0 and β . The parameters obtained from the above procedure are listed in Table II.

We used the above four-parameter sets for both compounds to estimate the intraband parts of the dielectric functions at higher energies (>1.2 eV). The intraband parts were subtracted from the ellipsometry data to get the interband parts. The ϵ_2^b for PtGa₂ obtained from the above procedure shows the structure at about 1.3 eV more developed than in Fig. 1. However, the ϵ_2^b s for both compounds still show increasing low-energy ends which might mean that there are strong interband transitions below 1.2 eV, the low-energy limit of our measurements. For this reason, the Drude parameters may not be meaningful for both compounds. They are used only to try to separate $\tilde{\epsilon}$ into two parts.

B. Band structures and optical transitions

Relativistic band structures of AuGa₂ and PtGa₂ including the spin-orbit interaction are shown in Figs. 3 and 4 along certain high-symmetry directions. In both structures, the bands near E_F are of Ga *s-p* character mixed with Au or Pt *s-p* character and these *s-p* bands along the $\Gamma-K$ and $L-W$ directions have quite similar shapes in the two materials except for the difference in E_F . Also, these bands do not shift much in energy by including the spin-orbit interaction as a perturbation while the lower-lying *d* bands shift and split significantly due to the combined spin-orbit and crystal-field effect.

The lowest band for both compounds consists of a mixture of Au 6*s*– or Pt 6*s*–Ga 4*s* bonding states. Its hybridization with 5*d* states of Au or Pt is much weaker than those in elemental Au or Pt. The narrow set of bands above this *s* band are 5*d* bands of Au or Pt. The positions of these 5*d* bands in AuGa₂ agree within 0.5 eV with the result of the angle-resolved photoemission measurement on the (100) surface of AuGa₂.³⁴ Also, the measured energy gap between Γ_7^+ and the lower Γ_8^+ from the above measurement is 1.6 eV while our calculation gives 1.1 eV. In PtGa₂ these 5*d* bands are located at higher energies than in AuGa₂: the upper Γ_8^+ is located 2.3 eV higher in PtGa₂ than in AuGa₂ relative to E_F . In Table III a comparison is made between the 5*d* states at Γ with and without the spin-orbit interaction for both compounds. It is seen that the widths of the 5*d* bands are increased due to the rise of the doubly degenerate $\Gamma_{12}(e_g)$ level to Γ_8^+ and also due to the splitting of the triply degenerate $\Gamma_{25}'(t_{2g})$ level into the twofold Γ_7^+ and fourfold Γ_8^+ . The width of the 5*d* bands estimated from the DOS

TABLE II. Drude parameters for AuGa₂ and PtGa₂ used to estimate the intraband part of the dielectric function.

Compound	ϵ_∞	$\hbar\omega_p$ (eV)	τ_0 (10^{-14} sec)	β (10^{14} sec ⁻¹ eV ⁻²)
AuGa ₂	2.70	4.72	0.602	10.2
PtGa ₂	4.94	6.29	1.27	5.38

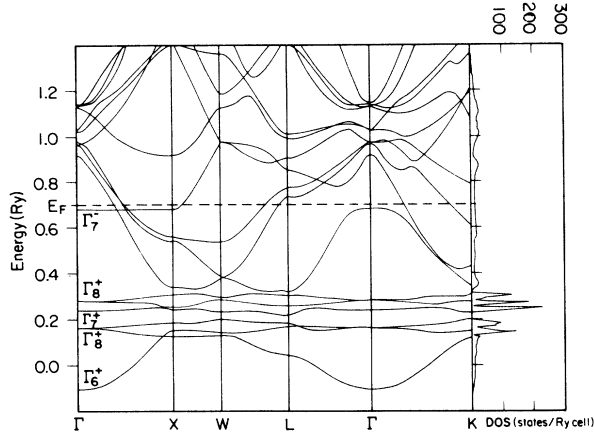


FIG. 3. Relativistic energy-band structure and density of states of AuGa₂ including spin-orbit coupling.

of AuGa₂ in Fig. 3 agrees well with the result of the valence-band x-ray photoemission spectroscopy (XPS) measurement.^{35,36}

The main difference between the band structures of AuGa₂ and PtGa₂ near E_F is that for AuGa₂ the band originating from the Γ_7^- is located below E_F along the $\Gamma-X$, $\Gamma-K$, and $\Gamma-L$ directions while for PtGa₂ it is above E_F along the $\Gamma-X$ direction and partially unfilled along the $\Gamma-K$ and $\Gamma-L$ directions. This band is derived mostly from Ga 4s antibonding states among neighboring Ga atoms. In AuGa₂, this band is quite flat along the $\Gamma-X$ direction and located 0.26 eV below E_F at the Γ point. However, this band does not cause a high density of states at about 0.26 eV because it disperses significantly in the other directions of the Brillouin zone. In other calculations,^{7,13} this band lies at lower energies and at the Γ point it is located about 1.4 eV below E_F , differing from our result by more than 1 eV.

We calculated the interband contribution to the imaginary part of the dielectric function ϵ_2^b for both AuGa₂ and PtGa₂ according to Eq. (5), including the effect of the

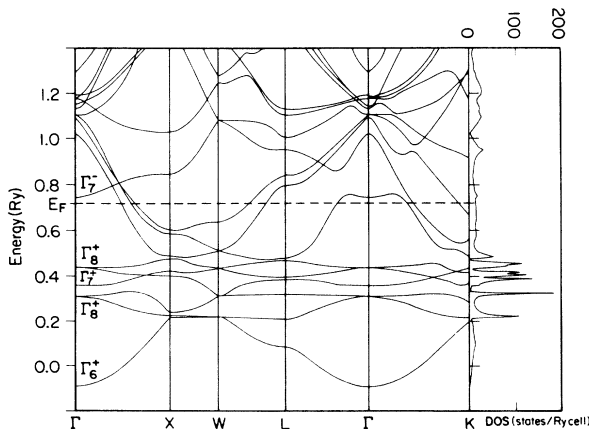


FIG. 4. Relativistic energy-band structure and density of states of PtGa₂ including spin-orbit coupling.

TABLE III. States at Γ for AuGa₂ and PtGa₂ with and without spin-orbit splitting. Zero energy refers to the muffin-tin zero.

AuGa ₂			
$E_F = 0.6980$			
non-s.o.		s.o.	
$\Gamma_{12}(e_g)$	0.2556	$\Gamma_8^+ (j = \frac{3}{2})$	0.2801
$\Gamma'_{25}(t_{2g})$	0.2049	Γ_7^+	0.2388
		$\Gamma_8^+ (j = \frac{5}{2})$	0.1613
PtGa ₂			
$E_F = 0.7160$			
non-s.o.		s.o.	
$\Gamma_{12}(e_g)$	0.4246	$\Gamma_8^+ (j = \frac{3}{2})$	0.4366
$\Gamma'_{25}(t_{2g})$	0.3363	Γ_7^+	0.3601
		$\Gamma_8^+ (j = \frac{5}{2})$	0.3101

electric dipole matrix elements. In Figs. 5 and 6 we compare our calculation results with the spectra obtained after subtracting the Drude-model calculations from the optical data. We can see that overall agreement is good between the two quantities for both the peak positions and the strengths of the structures for both compounds in our ellipsometry data range (1.2–5.5 eV). An interesting result is that both compounds show strong calculated interband absorptions below our ellipsometry data range: for AuGa₂ there is a peak at 0.65 eV, and for PtGa₂ there is a peak at 0.97 eV. At 1.2 eV, the strength of this interband absorption compared to the total absorption strength ϵ_2^b/ϵ_2 is 86% for AuGa₂ and 66% for PtGa₂. The reflectivity data of Wieliczka *et al.*²⁹ for both compounds do not show any structure at energies below 1 eV so that the dielectric functions obtained from them do not show any structure related to the interband absorptions in this range. This is possible if the strengths of the

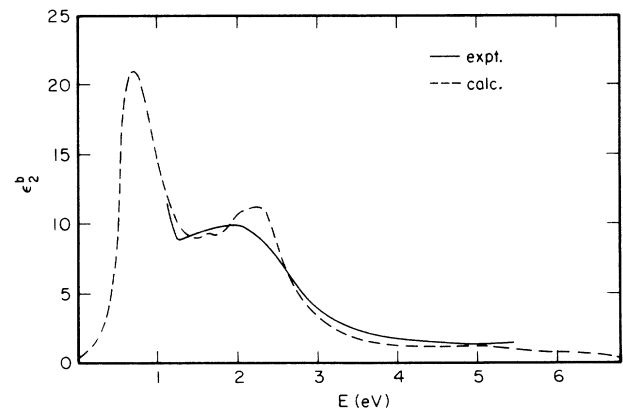


FIG. 5. Comparison of the interband contribution to the imaginary part of the complex dielectric function for the band calculation (broadened by convolution with a Lorentzian of full width at half maximum of 0.05 eV) and the experiment for AuGa₂.

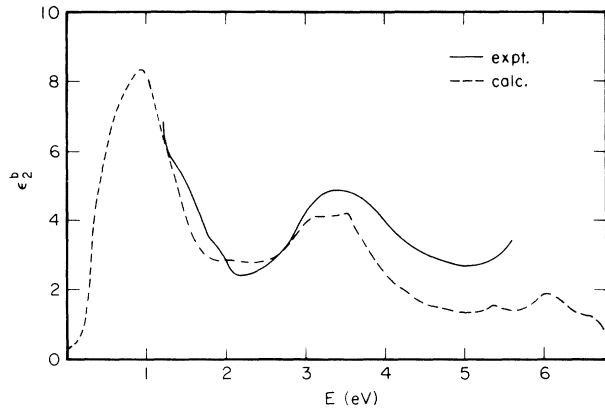


FIG. 6. Comparison of the interband contribution to the imaginary part of the complex dielectric function for the band calculation (broadened by convolution with a Lorentzian of full width at half maximum of 0.05 eV) and the experiment for PtGa₂.

intraband absorptions at room temperature are much greater than those of the interband absorptions so that the reflectivity measurements could not resolve the weaker interband contributions from the stronger intraband contributions. Another possibility is that our calculations might overestimate the strengths of the low-energy interband absorptions, or place them slightly too high in energy, where they would appear to be more observable. By calculating the interband contribution to ϵ_1 from our calculated interband ϵ_2 , adding these to the Drude $\tilde{\epsilon}$, and calculating the reflectivity, we find no detectable structure in reflectivity is expected in PtGa₂ due to the low strength of these interband transitions. Such a structure should be detectable in AuGa₂ if the calculations are accurate.

As a good example, the reflectivity measurement on Al (Ref. 37) at room temperature could not resolve a structure due to the interband absorption at low energies (< 1 eV) from the background of intraband absorption. Also, KK analysis³⁹ using various room-temperature optical data, including the above, could not produce the low-energy structure. However, an absorptivity measurement on Al at 4.2 K (Ref. 39) showed an interband absorption peaked at about 0.5 eV. Therefore, for some metals, phonon-assisted intraband absorption might increase dramatically as the temperature rises so that at room temperatures we might not resolve the interband absorptions at low energies.

To find the regions in k space which contribute significantly to the structures in ϵ_2^b we calculated the integral part of Eq. (5) for each of the 110 tetrahedra for selected energy windows centered at about the peaks of each structure for both compounds. The intensities of all the interband transitions having energy differences between the initial and final states falling in the energy window were summed for each tetrahedron to represent the contribution from the tetrahedron to the structure. In Figs. 7 and 8 each tetrahedron is represented by a rectangle if it makes a contribution to the structure, with the

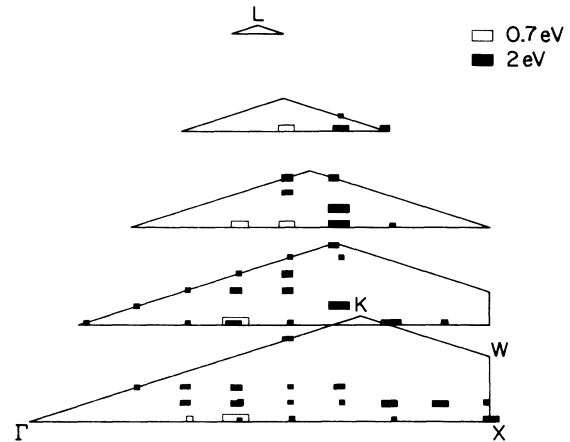


FIG. 7. Regions in the irreducible wedge of the Brillouin zone of AuGa₂ contributing to interband transitions in the 0.61–0.75-eV and 1.9–2.1-eV spectral region. Larger rectangles show the locations of the small tetrahedra with the larger contributions (from the product of dipole-matrix elements and joint density of states). Smaller rectangles show weaker transitions.

size of the rectangle denoting the strength of the contribution. Figure 7 shows the distribution of the transitions for the 0.65-eV peak of AuGa₂ in the $\frac{1}{48}$ th of the Brillouin zone. The largest contribution comes from around the middle of the Γ - X line. These transitions occur between bands having mostly s - p character. As shown in Fig. 3 there are three nearly-parallel bands along the Γ - X direction. The lowest band of the three at the X point (band 8) has Au s - p character and the other two upper bands (bands 9 and 10, respectively) have mixtures of Au p and Ga p character at around the middle of the Γ - X line. The 0.65-eV peak is caused primarily by transitions between bands 8 and 9. At about 1 eV the strength of the transitions between bands 8 and 10 is comparable to that

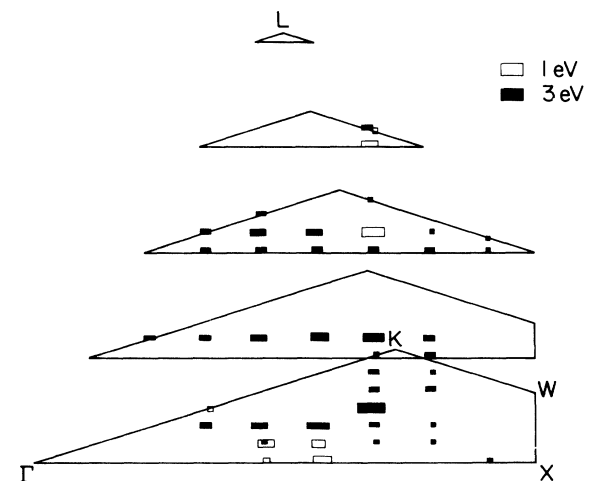


FIG. 8. Regions in the irreducible wedge of the Brillouin zone of PtGa₂ contributing to interband transitions in the 0.88–1.02-eV and 2.9–3.1-eV spectral region.

of the transitions between bands 8 and 9 so that a small shoulder occurs on the falling slope of ϵ_2^b in Fig. 5. Figure 8 shows the distribution for the 0.97-eV peak of PtGa₂. The largest contribution comes from the region between the middle of the $\Gamma-X$ line and the middle of the $\Gamma-K$ line in the ΓXWK plane. As can be seen in Fig. 4 the band structure of PtGa₂ along the $\Gamma-X$ direction also has three nearly parallel bands. Giving the same indices to these bands as those in AuGa₂, band 8 has Pt *s-p* character and bands 9 and 10 have mixtures of Pt *p-d* and Ga *p* character. In PtGa₂ the *d* bands of Pt are located higher than those of Au in AuGa₂ so that the bands near E_F have significant *d* character through the hybridization. The strength of the 0.97-eV peak is mainly due to transitions between bands 8 and 9. The strength of the transitions between bands 8 and 10 grows as the energy increases to make a shoulder at about 1.3 eV in ϵ_2^b of PtGa₂. The contributions to the 2-eV structure of AuGa₂ are throughout nearly all of the irreducible wedge and the contribution from the high-symmetry regions is very small compared to the total strength, as can be seen in Fig. 7. These contributions come mainly from transitions between filled bands having mixtures of Au *p* and Ga *p* character (like bands 9 and 10 along the $\Gamma-X$ direction) and unfilled bands having Ga *s-p* character. Figure 8 shows the contributions to the 3-eV structure of PtGa₂. The contributions occur throughout all of the irreducible

wedge. These transitions are mostly between the filled bands with Pt *s-p* character and the unfilled bands with Pt *p-d* character mixed with Ga *p* character.

V. CONCLUSIONS

The optical properties of intermetallic compounds AuGa₂ and PtGa₂ in the 1.2–5.5-eV region agree well with the results from relativistic band-structure calculations including the spin-orbit interaction in the absolute magnitudes as well as the positions of the structures. Below 1.2 eV the calculational results for both compounds exhibit peaks which are due to transitions involving unfilled bands having Ga *p* character. The interband terms ϵ_2^b for both compounds also show rising trends at low energies which may be evidence for the existence of the above-mentioned transitions below 1.2 eV as in the case of Al.

ACKNOWLEDGMENTS

The authors would like to thank Dr. D. M. Wieliczka for providing the reflectivity data. The Ames Laboratory is operated for the U.S. Department of Energy by Iowa State University under Contract No. W-7405-Eng-82. This work was supported by the Director for Energy Research, Office of Basic Energy Sciences, U.S. Department of Energy.

*Present address: Department of Electrical Engineering, University of Nebraska-Lincoln, Lincoln, NE 68588-0511.

¹J.-P. Jan and W. B. Pearson, *Philos. Mag.* **8**, 279 (1963).

²J.-P. Jan, W. B. Pearson, Y. Saito, M. Springford, and I. M. Templeton, *Philos. Mag.* **12**, 1271 (1965).

³J. T. Longo, P. A. Schroeder, and D. J. Sellmyer, *Phys. Rev.* **182**, 658 (1969).

⁴S. S. Vishnubhatla and J.-P. Jan, *Philos. Mag.* **16**, 45 (1967).

⁵K. E. Saeger and J. Rodies, *Gold Bull.* **10**, 10 (1977).

⁶L.-Y. Chen and D. W. Lynch, *Phys. Status Solidi B* **148**, 387 (1988).

⁷A. C. Switendick and A. Narath, *Phys. Rev. Lett.* **22**, 1423 (1969).

⁸N. E. Christensen, *Phys. Rev. B* **13**, 2698 (1976).

⁹R. Lässer, N. V. Smith, and R. L. Benbow, *Phys. Rev. B* **24**, 1895 (1981).

¹⁰H. Eckardt, L. Fritsche, and J. Noffke, *J. Phys. F* **14**, 97 (1984).

¹¹K. A. Mills, R. F. Davis, S. D. Kevan, G. Thornton, and D. A. Shirley, *Phys. Rev. B* **22**, 581 (1980).

¹²R. Courths, H. Wern, U. Hau, B. Cord, V. Bachelier, and S. Hüfner, *J. Phys. F* **14**, 1559 (1984).

¹³S. Kim, J. G. Nelson, and R. S. Williams, *Phys. Rev. B* **31**, 3460 (1985).

¹⁴G. P. Pells and M. Shiga, *J. Phys. C* **2**, 1835 (1969).

¹⁵R. Rosei and D. W. Lynch, *Phys. Rev. B* **5**, 3883 (1972).

¹⁶S. Kim, L.-S. Hsu, and R. S. Williams, *Phys. Rev. B* **36**, 3099 (1987).

¹⁷D. D. Koelling and B. N. Harmon, *J. Phys. C* **10**, 3107 (1977).

¹⁸J. Callaway and C. S. Wang, *Phys. Rev. B* **7**, 1096 (1973).

¹⁹R. J. Baughman, *Mater. Res. Bull.* **7**, 505 (1972).

²⁰L.-Y. Chen and D. W. Lynch, *Appl. Opt.* **26**, 5221 (1987).

²¹D. Liberman, J. T. Waber, and D. T. Cromer, *Phys. Rev.* **137**,

27 (1965).

²²L. Hedin and B. I. Lundqvist, *J. Phys. C* **4**, 2064 (1971).

²³V. L. Moruzzi, J. F. Janak, and A. R. Williams, *Calculated Electronic Properties of Metals* (Pergamon, New York, 1978).

²⁴D. J. Peterman, B. N. Harmon, J. Marchiando, and J. H. Weaver, *Phys. Rev. B* **19**, 4867 (1979).

²⁵T. A. Tibbetts and B. N. Harmon, *Solid State Commun.* **44**, 1409 (1982).

²⁶Y. Chen, K. M. Ho, and B. N. Harmon, *Phys. Rev. B* **37**, 283 (1988).

²⁷O. Jepsen and O. K. Anderson, *Solid State Commun.* **9**, 1763 (1971).

²⁸M. Ellner, U. Kattner, and B. Predel, *J. Less-Common Met.* **87**, 305 (1982).

²⁹D. M. Wieliczka, A. Nienhueser-Duppe, and D. Striley (unpublished).

³⁰J. B. Smith and H. Ehrenreich, *Phys. Rev. B* **25**, 923 (1982).

³¹K. J. Kim, L.-Y. Chen, and D. W. Lynch, *Phys. Rev. B* **38**, 13 107 (1988).

³²R. T. Beach and R. W. Christy, *Phys. Rev. B* **16**, 5277 (1977).

³³G. R. Parkins, W. E. Lawrence, and R. W. Christy, *Phys. Rev. B* **23**, 6408 (1981).

³⁴J. G. Nelson, W. J. Gignac, S. Kim, J. R. Lince, and R. S. Williams, *Phys. Rev. B* **31**, 3469 (1985).

³⁵S. Hüfner, J. H. Wernick, and K. W. West, *Solid State Commun.* **10**, 1013 (1972).

³⁶P. M. Attekum, G. K. Wertheim, G. Crecelius, and J. H. Wernick, *Phys. Rev. B* **22**, 3998 (1980).

³⁷H. E. Bennett, M. Silver, and E. J. Ashley, *J. Opt. Soc. Am.* **53**, 1089 (1963).

³⁸E. Shiles, T. Sasaki, M. Inokuti, and D. Y. Smith, *Phys. Rev. B* **22**, 1612 (1980).

³⁹L. W. Bos and D. W. Lynch, *Phys. Rev. Lett.* **25**, 156 (1970).